
Article:
Stone, E.J.W., Panagiotou, P.A., Mühlthaler, J. et al. (2026) Thermal failure of stator winding insulation and useful life assessment by impedance spectroscopy. IEEE Transactions on Industry Applications. ISSN: 0093-9994

https://doi.org/10.1109/tia.2026.3656154

Thermal Failure of Stator Winding Insulation and Useful Life Assessment by Impedance Spectroscopy

Edward J. W. Stone, Panagiotis A. Panagiotou, *Member, IEEE,* Johannes Mühlthaler, *Member, IEEE,* Andrew R. Mills, Alexis Lambourne, and Geraint W. Jewell

***Abstract*—This paper presents a novel application of impedance spectroscopy as a means of inspection for stator winding insulation degradation identification. It proposes, for the first time, a tool for health monitoring and failure identification during thermal degradation effects in the insulation systems of stator coils from a concentrated stator winding. By periodical ex-situ inspection of these coils, the thermal ageing data of the insulation are profiled until the point of failure. The study maps this evolution of the thermal degradation pattern via novel interpretation of the differential-mode impedance frequency responses, using well known techniques such as the Bode and Nyquist plots. This grants further insight into the characteristics shown in the ageing profiles over time and frequency. These thermal failure profiles enable the identification of critical points that can act as pre-emptive indicators of coil health and failure inception. This is a key finding as it renders the capability to provide an adequate lifespan tool for electrical machine concentrated windings and coil assemblies in terms of remaining useful life and failure interpretation. The insulation system examined in this study is from the coils of the concentrated stator winding of a 2MW permanent magnet generator used in an aerospace application.**

***Index Terms*—Stator winding health, Coil Failure, Insulation degradation, Impedance Spectroscopy, Thermal Aging**

I. Introduction

WITH the need for greener alternatives to meet low emission targets, electrified transportation is a rapidly expanding sector in market growth, research, and innovations. Therefore, electrical machines have made significant inroads in traction applications and aviation [1]-[3]. Amongst the various components of electrical machines, insulation systems are continuously attracting increased research interest as they are one of the key components relating to safety, failure mitigation, and machine efficiency. These systems have a critical role in the lifespan of electrical machines and electric drives with respect to thermal management, protection, and stress endurance [3]-[5]. Stress factors have a direct influence on the degradation of the several layers in the insulation system. This degradation results in fault initiation with severe safety and financial risk [6]-[7]. Therefore, it is vital to detect, localise, and diagnose insulation faults timely with adequate warning time to mitigate a failure.

Several technologies have been developed in this field, spanning aspects in testing procedures, inspection techniques, and monitoring methods. The application of in-service continuous condition monitoring of the electrical machine is one of the aspects pertaining to this research [7]-[10]. Although these fault detection methods work reliably for several types of faults, they have shown significant limitations in terms of fast response for failure alerts. This makes insulation failures even more challenging, as defects in the insulating materials can cause rapidly evolving short circuit faults that can damage the machine within a few minutes. With respect to insulation monitoring, several published works have contributed to the advancement of this field. By way of examples, one novel scheme for partial discharge (PD) monitoring was reliably implemented recently in [12], while measurements of the common mode voltage and impedance were shown in [13] and [14] respectively for the adequate health monitoring of insulation. Experimental testing by measurements and analysis of the broadband common-mode impedance spectrum was also shown to reliably diagnose interturn and ground wall insulation ageing in [15]. However, insulation monitoring requires fine resolution in terms of instrumentation and bandwidth capabilities incurring significant costs on the monitoring system. For most cases, a combination of sensing methods is needed to ensure reliability of on-board diagnostics that require a plethora of sensors and costly instrumentation [16]-[19].

Prior to in-service monitoring, stator windings and their insulation systems are subjected to factory acceptance testing after manufacturing stages by IEEE/IEC standards and safety regulations [7]. Further testing takes place upon the pre and post machine assembly stages for compliance with functional requirements and quality assurance. Such tests encompass a

This work was supported by the Aerospace Technology Institute (ATI UK) and Innovate UK/UKRI under the project REPLENISH (Grant 10112182).

Corresponding author: Panagiotis A. Panagiotou

E. J. W. Stone is with the School of Electrical and Electronic Engineering, University of Sheffield, S1 3JD, Sheffield, U.K., (e-mail: e.j.stone@sheffield.ac.uk).

P. A. Panagiotou is with the School of Electrical and Electronic Engineering, University of Sheffield, S1 3JD, Sheffield, U.K. (e-mail: p.panagiotou@sheffield.ac.uk).

J. Mühlthaler is with the School of Engineering and Design, Technical University of Munich (TUM), 85748, Garching, Germany (e-mail: johannes.muehlthaler@tum.de).

A. R. Mills is with the School of Electrical and Electronic Engineering, University of Sheffield, S1 3JD, Sheffield, U.K. (e-mail: a.r.mills@sheffield.ac.uk).

A. Lambourne is with Rolls-Royce Central Services, Rolls-Royce Plc UK, DE24 9HY, Derby, U.K. (e-mail: Al.Lambourne@rolls-royce.com)

G. W. Jewell is the School of Electrical and Electronic Engineering, University of Sheffield, S1 3JD, Sheffield, U.K. (e-mail: g.jewell@sheffield.ac.uk).

variety of methods and techniques, including insulation resistance measurements, surge testing, dielectric withstand testing, high potential testing (HiPOT), etc. In-depth reviews elaborating on the discussed testing methods are provided with detail in [6], [7], [11], and [18]-[20]. Nevertheless, there is a considerable body of the literature that arguably criticises many of these testing protocols. The rationale is the fact that although these tests reveal valuable diagnostic indexes and information regarding health condition, they are limited to pass/fail decisions rather than fault localisation or actual estimation of remaining useful life. Concurrently, these testing procedures impose high stresses on the materials with questionable impact on the insulating system or component under test with regards to the consumption of remaining insulation loading capacity and useful life due to the stresses of the testing conditions.

Over the electrical machine lifespan, testing for purposes of on-wing and off-wing periodical inspection is performed using several sensing methods and novel instrumentation. Electrical impedance spectroscopy (EIS) is an inspection method utilising the measurement of the insulation system impedance to allow its characterisation by the response of the impedance function over a broad frequency range [17]. EIS evolved from prior techniques such as dielectric spectroscopy and electrochemical impedance spectroscopy and became more established as a practical measurement due to its simplicity, applicability, and non-destructive nature [17], [21]. Several published studies on the application of EIS have exploited its applicability for testing and diagnostic inspection purposes. Nevertheless, EIS is mainly applied as ex-situ means of inspection and has limited application in-situ due to several reasons including ease of access to the winding terminals, instrumentation volume and weight, and level of sensitivity to machine elements, e.g., the machine iron core, or neighbouring rotor components such as the magnets in PM machines. However, its applicability, versatility, and non-destructive nature make it a very promising technology suitable for strategies incorporating lineside inspection, health assessment, and life prediction tools.

In this paper, a novel application of differential-mode EIS is utilised as a means of ex-situ inspection and health assessment of thermally aged coils from a concentrated stator winding. The winding is from the stator of a 2MW generator deployed in the hybrid architecture of an aircraft demonstrator [17], [21]-[26], [27]. Thus far, published insulation monitoring techniques are currently limited with respect to the complete thermal degradation mapping until a confirmed point of coil failure. The examined coils were thermally aged at a temperature slightly above the rated for this insulation class, emulating gradual ageing effects. The paper demonstrates an extension of the work presented in [21] and [28], with emphasis on a new concept of insulation degradation and failure profiling. Here, the trend lines derived from tracking the maximum impedance value over frequency, identify for the first time the insulation system thermal failure points for concentrated stator coils with enamel wire (Litz) bundles of strands making up the coil turns. These failure points are validated using well-established EIS representations, such as Bode plots and Nyquist locus. The findings of this work contribute to the existing body of research, by adding the value of mapping the complete thermal degradation profile of an insulation system from its start of life up until electrical failure of the coil due to thermal degradation. This methodology for identification of critical failure points provides a tool to threshold and facilitate failure warnings that can alert for mitigation actions. Further, an additional contribution of this work is the foundation of a lifespan tool by the combination of the identified thresholds with the impedance Nyquist responses. Key contributions of the presented work's findings include profiling the complete coil insulation system's thermal degradation up to the point of coil failure, while capturing and mapping the thermal failure incident. These are followed by the identification of critical failure points by the impedance trend reversal and the interpretation of the failure via theoretical analysis; this is further validated by intrinsic coil inspection using CT imaging that show the changes within a coil structure's areas that are linked to the thermal failure mechanism.

II. Stator Winding Insulation & Inspection by EIS

A. Insulation Stresses & Failures

The stress factors experienced by the electrical machine insulation system have several origins generating what are referred to as T.E.A.M. stresses (thermal, electrical, ambient, mechanical) [7], [20]-[21]. Their distribution and impact directly relate with application related requirements, notably environmental conditions, and mission profile during operation. For example, in terrestrial traction applications electrical machines experience intense vibrations, torque profiles and currents with transient dynamics, and frequent start-stops. These result in intensified mechanical and electrical stresses and periodical thermal overloads that are highly likely to create weak spots on or within the insulation layers. Aerospace applications are even more challenging due to the increased environmental and application constraints. The key factors are mechanical stresses from vibrations, electrical stresses like PD due to reduction of the inception voltage at high altitudes with low pressure, and thermal stresses due to high currents and voltages with converter switching [7], [19], [22], [25], [29].

Such adverse conditions and intensified stresses initiate the ageing of the insulation, accelerating failure mechanisms. As degradation of the insulation layers progresses, the profile of the insulation system with respect to structural, electrical, and material properties is continually changing. The repercussion is the creation of a local defect at very low severity leading to an undetectable fault at incipient level [30]-[31]. Although such faults are initially localised in a small fraction of the insulation layer, they impose gradual damage on the insulation system resulting in accelerated ageing. Eventually, this situation leads to a severe fault that will cause in-service failure of the machine inflicting costs and safety risks [31]-[33].

Thermal stresses form the most significant factor incurring degradation and failures in electrical machine insulating systems. They are directly related to mechanical stresses from vibrations and noise as well as electrical stresses due to high

currents, voltage surges, and PD [2], [7], [20], [34]. A vast amount of research in the literature is investigating the ageing of insulation materials and systems focusing mainly on accelerated thermal ageing, thermal cycling, estimation of remaining useful life, and insulation breakdown in several different conditions [35]-[42]. These include studies with measurements for direct condition monitoring, statistical evaluation, etc. The failure rate of insulation samples or winding components observed in such studies varies from 600 to 2600 hours of ageing, depending on the type and conditions of the emulated stresses. The reason for this broad range of values is the acceleration of ageing by different factors during the stressing process. During this acceleration, the alteration of the ageing profile has a variable pattern that relates to the structure of the component under test and its materials, the conditions of testing, and the emulated multi-stress effect [7], [20]-[21]. With a plethora of forced accelerated ageing there is novel room within the state of the art for a true understanding of a coil life span under more realistic thermal degradation scenarios. The purpose of this study is to map the effects of thermal ageing at only 20°C above the rated temperature for the insulation class. This small increase accounts for a realistic exposure at temperatures that can occur during operation, either by additional heat from electrical stresses or due to environmental factors surrounding the coils.

B. Coil Inspection & Electrical Impedance Spectroscopy (EIS)

As discussed in the introduction, EIS measurements have rendered valuable results for material characterisation and health condition assessment. As an inspection method, EIS has been developing in tandem with other diagnostic approaches as a non-destructive method with promising potential for in-situ application. With regards to the evaluation of stator windings and components such as coil assemblies, EIS performs a frequency sweep to measure the function of the global impedance $Z(\omega)$ over the frequency spectrum:

$$Z(\omega) = |Z| \angle \varphi = Re\{Z\} + j \cdot Im\{Z\}, \quad (1)$$

where $|Z|$ is the impedance amplitude, φ the phase angle, while $Re\{Z\}$ and $Im\{Z\}$ express the real and imaginary part of the complex impedance, respectively, with R and L being the total coil resistance and inductance, respectively:

$$\mathrm{Re}\{Z\} = \omega / [(1 - \omega^2 CL)^2 + (\omega RC)^2], \quad (2)$$

$$Im\{Z\} = \omega(L - R^2C - \omega^2CL^2)/[(1 - \omega^2CL)^2 (\omega RC)^2] \quad (3)$$

During EIS measurements, the amplitude and angle terms shown in (1) are analysed and evaluated for the identification of the resonant frequencies and peak impedance in the Bode plots [17], [43]-[49]. The natural, undamped resonant frequency $f_0 = 1/[(2\pi)(LC)^{1/2}]$ defines the frequency f_{max} at which the impedance magnitude becomes maximum [27].

As explained in [17] and [21] using EIS for the ex-situ periodical inspection of these coils, thermal ageing has a direct influence with tangible effect on the amplitude term of (1), and negligible effect on the angle term. In terms of novel inspection, the key effect of thermal degradation is the increase of the peak impedance with the progression of thermal ageing in tandem with a shift of the frequency f_{max} towards higher ends of the spectrum in the Bode plots. These observations are validated by the behaviour of the impedance Nyquist plots, where the locus of the terms of (2) and (3) are examined. This paper states that in these plots it was seen that; although the impedance locus retains the same circular or elliptical shape over the ageing timeline, the degradation effect was responsible for expanding the impedance locus with the progression of the ageing. With the angle term measured nearly constant in the Bode plots over ageing, this Nyquist expansion directly reflects the increasing trend of the amplitude due to the increase of the terms described by (3). By the discussed rationale, the next section presents a novel utilisation of this methodology using an EIS-based strategy to enable the detection of critical points pertaining to the failure of the insulation system. The identification of these failure points is supported by the impedance extrema in the Nyquist locus, which reverses the profile of its trendline followed by gradual drops in the maximum impedance tracking of the Bode plots from the critical point onwards.

III. Experimental Methodology & Test Hardware

The coils from the concentrated stator winding of a 2 MW generator have been used in this study. The stator coils are shown in Fig. 1a. A cross section of the coil side and the individual insulation layers are shown in Fig. 1c. This is a Class H (180°C) insulation system, as also described in [21] where the initial degradation rate of this insulation system was investigated at the early stages of ageing. Each coil side consists of 8 turns made of PAI-coated enamel wire bonded in bundles of 350 strands with encapsulation varnish in between. The bundle turns are surrounded by several insulation layers, illustrated in Fig. 1b under microscope view with a ×50 magnification. Figure 1b depicts the strand insulation of the enamel wire components in a coil at two different instances, at the start-of-life and at 3000 hours of thermal ageing.

a) **b)**

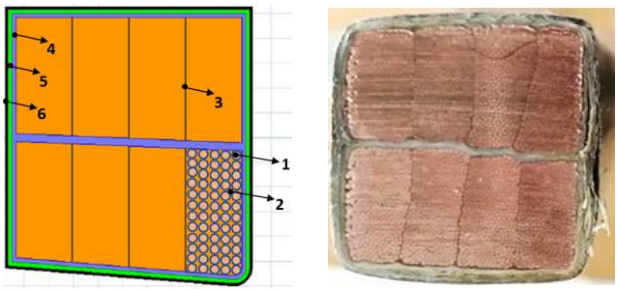

c) d)

Fig. 1. Stator coils examined in the thermal ageing study: a) Set of coil assemblies, b) Microscope view (×50 magnification) of the strand insulation of the enamel wire in the coil at the start-of-life stage (top) and after 3000 hours of thermal ageing (bottom), c) Components of a coil insulation system, d) Cross-section of one of the coil sides.

The coils were thermally aged at 200°C up to 5600 hours using the ovens shown in figure 2a and 2b in cycles of 100 hours, as described in [21]. After each 100-hour interval, they were inspected by differential-mode EIS to collect the impedance at every 100-hours ageing point. For the measurements, the impedance analyser WK–1J6500B was used, shown in figure 2b. The measurements were taken at the coil terminals (tap points), hence evaluating the overall insulation health of a coil structure under test by differential-mode impedance spectroscopy. The data collated every 100 hours were taken after allowing the coils to settle at room temperature and then analysed and profiled by the Bode plots for tracking the peak impedance changes with respect to the resonance frequency changes and the overall degradation time. As final step, the locus of the impedance Nyquist plots was used to validate the changes as well as the identified failure points of each coil after more than 5500 hours of thermal ageing.

(a) (b) (c)

Fig. 2. Thermal degradation setting and instrumentation: a) Oven to thermally degrade the examined coils, b) Coils assemblies in the degradation oven, c) Impedance analyser used for the EIS measurements.

With the coil voltage rating at 1.6 kV, two sets of HiPOT testing were performed as in factory acceptance testing stage, at twice the rated voltage +1kV as set out in the related standards for this type of testing IEC 60034-27-1, IEC 60034-27-3, IEC 60034-15 [50]-[52]. The first HiPOT test was performed at 4000 hours of thermal ageing and indicated a clear pass outcome for all the coils. The second HiPOT test was performed on each coil after the first point of failure identified by the presented analysis. In both cases, the effect of the high potential testing did not affect the impedance response of the coils with any degradation rate compared to the tangible effect of thermal ageing in shifting the peak impedance values towards a higher resonance frequency range.

IV. Results and Discussion

A. Identification of Critical Failure Points by Peak Impedance Tracking & Degradation Profiling

The impedance response measurements over frequency are shown in Fig. 3 for coil C1. The responses of magnitude and phase over the complete sweep's spectrum are shown in Fig. 3a and Fig. 3b, respectively, at the thermal degradation instances of 0 hours (black curve, start of life), 2000 hours (red), 4000 hours (yellow), 5100 hours (blue) and 5600 hours (green). Furthermore, Fig. 3c focuses in the frequency zone of the first resonance peak for all hours of thermal ageing, with each curve from left to right representing every 100 hours of exposure to thermal ageing along the x-axis. As also described in [21] and [28], there is a clear monotonic increase of the peak impedance with the progression of thermal ageing in tandem with an increasing trend in the shifting of the frequency f_{max} towards higher ends of the spectrum. The values of the peak impedance corresponding to the frequency response peaks of Fig. 3c are shown in Table I up to the point of obsolete failure for the examined coils. The values in Table I and impedance peaks shown in Fig. 3c at each resonance frequency shift validate through equations (2)-(3). The results of the measured frequency responses shown through all subfigures of Fig. 3 illustrate one of the examined coils (C1) for demonstration purposes by a representative coil from the examined batch, as all the other coils of this type and manufacture show similar behaviour in their responses and trend.

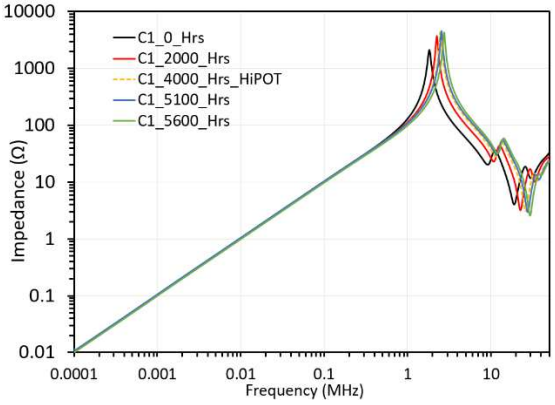

a)

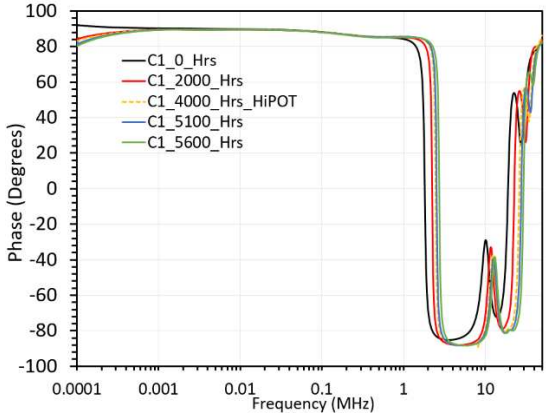

b)

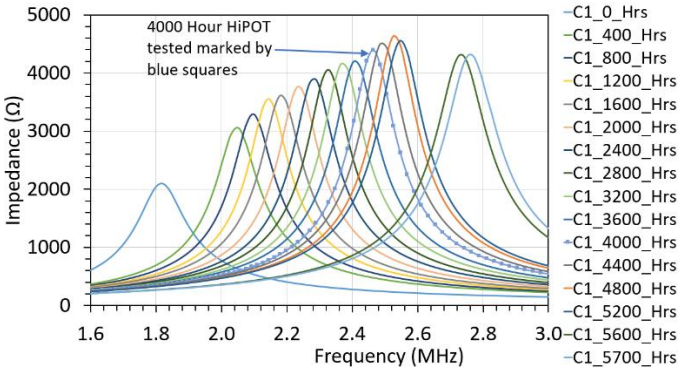

c)

Fig. 3. Impedance sweep frequency response analysis (SFRA): a) magnitude plot (|Z| vs. frequency *f*), b) phase plot ($\angle Z$ vs. *f*), c) peak impedance tracking showing the changes in the impedance amplitude versus the resonance frequency shift in coil C1 from 0 to 5800 hours of thermal ageing.

TABLE I
IMPEDANCE AMPLITUDE PER COIL FOR THERMAL AGEING FROM 0-5800 HOURS AT THE RESONANCE FREQUENCY ω_{max}

	Coil Impedance Amplitude (kΩ)			
Hours	C1	C2	C3	C4
0	2.1	2.1	2.24	2.48
400	3.05	2.95	2.99	3.49
800	3.29	3.28	3.32	3.99
1200	3.55	3.49	3.47	4.19
1600	3.61	3.63	3.62	4.3
2000	3.77	3.77	3.78	4.49
2400	3.88	3.78	3.78	4.46
2800	4.06	3.87	3.92	4.56
3200	4.15	4.02	4.06	4.59
3600	4.2	4.13	4.19	4.76
4000	4.4	4.28	4.36	4.96
4400	4.5	4.37	4.45	5.07
4800	4.63	4.39	4.38	4.78
5200	4.56	4.44	4.42	
5600	4.3	4.4	4.31	
5700		4.2		
5800				

The key objective is to extract the comparative trendline of these peaks with respect to the degradation time and with respect frequency as shown in Fig. 4 and Fig. 5, respectively. Although the ageing data were collected every 100 hours, the results presented Fig. 3 and Table I are shown for every 400 hours for illustration clarity. The trendline of the peak impedance changes with respect to the hours of thermal ageing is shown in Fig. 4 for all coils. The black colour represents C1, while blue, red, and green represent C2, C3, and C4 respectively. Three zones of different profile trends are identified, labelled as "Zone #1", "Zone #2", and "Zone #3" in Fig. 4, marked by the vertical dashed lines. The area of Zone #1 indicates the start of life and the initial thermal ageing effect for an examined coil demonstrating a nearly exponential trend. The area of Zone #2 represents the degradation profile curve over the span of hours at temperature exposure demonstrating a linear trend in the impedance increase over the aging hours. As will be shown through Fig. 4 and 5, Zones #1 and #2 represent the overall coil useful life. Finally, Zone #3 represents the area where the degradation profile reverses towards a negative gradient indicating the critical point of failure and the end of the coil's useful life.

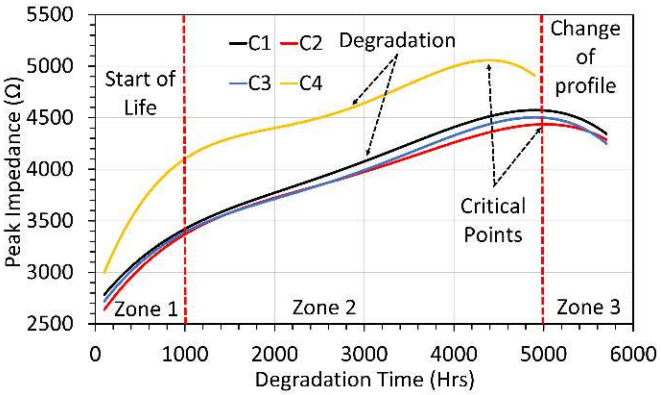

Fig. 4. Comparative plot of the thermal degradation profiles over time for all coils from 0 – 5700 hours of ageing: C1 (black), C2 (red), C3 (blue), C4 (yellow).

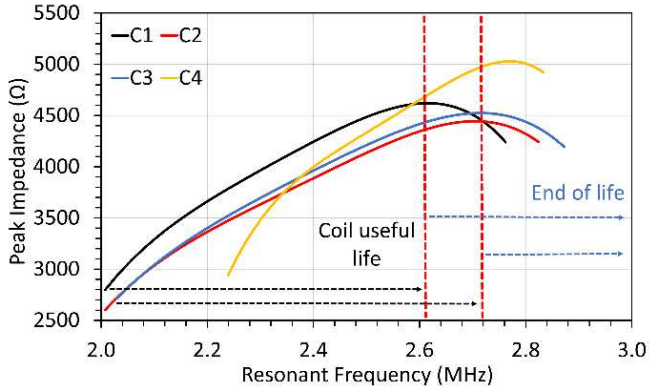

Fig. 5. Comparative plot of the thermal degradation profiles versus the resonance frequency for all coils from 0 – 5700 hours of ageing: C1 (Black), C2 (Red), C3 (Blue), C4 (Yellow).

While the profile transits from Zone #2 to Zone #3, this gradient becomes zero, thus allowing the identification of the critical points shown in Fig. 4. These points act as the key enablers for thresholds alerting for withdrawing from service or maintenance and repair action, as they are clearly signalling the initiation of thermal failure. By Fig. 4, C4 exhibits an outlier value with the peak impedance trendline being by an offset higher compared to the other three coils of this batch. This observation is expected, as C4 was characterised with a borderline pass outcome during factory acceptance testing and was later diagnosed as healthy with minor defects by EIS inspection at the earlier stages of this work presented in [17]. Despite this offset, C4 exhibits the same profile behaviour in terms of monotonic trend and gradient in

the impedance peak with the progression of the thermal ageing. Additionally, the high potential testing of C4 at 4000 hours rendered a pass outcome as in all the other coils of this study. These findings indicate that although minor defects may be present in the insulation system, the coil experiences the same thermal degradation rate with a completely healthy coil with respect to time. The differences observed are the offset in amplitude and the fact that the critical point for this coil appears only a few hours earlier than the other coils by 400-500 hours. The critical point for C1 occurred at 5600 hours, for C2 at 5700 hours, C3 at 5500 hours, and for C4 at 4800 hours of thermal ageing. As such, the useful life span of coils C1, C2, and C3 varies by an offset of 100-200 hours from each other, whereas C4 being minor defective reached its end-of-life state by the thermal failure at 4800 hours having an offset of 700-900 hours from the other three coils in the examined batch.

As mentioned, the ageing trendline with respect to frequency response is depicted in Fig. 5. It visualises the thermal degradation profile versus the resonance frequencies changes with the progression of the ageing. In a very similar trend with Fig. 4, the thermal ageing profile of Fig. 5 exhibits an increasing trend until the profile behaviour reverses. This indicates two distinguished zones of the coil ageing trendline. The first one is the linear increase area, labelled as coil useful life in Fig. 5, and includes the start-of-life and ageing curve with reference to Fig. 4. The second one is the end-of-life stage, marked by the critical points where the reverse profile behaviour is initiated in the same way with the critical points shown in Fig. 4.

Very similar observations are drawn from Fig. 5 with regards to the profile of C4, as it shows from its start of life slightly higher impedance and f_{max} values compared to the other coils. Nevertheless, the ageing profile of C4 follows a consistent trend over frequency with slightly higher gradient and increased f_{max} at the critical point. Due to its slightly defective nature by manufacture, the slope (gradient) of the C4 curve (yellow) in Zone #2 (useful life) is steeper than the other coils (C1, C2, C3), indicating a faster increase in impedance per unit frequency shift. This is due to the different frequencies exhibited in the impedance frequency response of C4, imposed by the coil resonance frequencies –which are slightly altered in C4 due to the inherent anomaly identified during factory acceptance testing. Similar with the identified critical points in Fig. 4, the critical points of changing profile with respect to frequency provide a pre-emptive indicator for signalling the need of actions such as maintenance and service requirement, stator winding repair or replacement, or refurbishment -all of which are significant aspects of the machine lifecycle. It is clear to see in Table I that the unaged baseline result and the critical point of failure are just over two times the impedance value; C1 at 2.2 times, C2 at 2.1 times, C3 at 2.0 times and C4 at 2.0 times. This suggests a key point of interest to identify thermal failure points for the inspected coils, which potentially allows to set an empirical threshold with regards to when the peak impedance in the EIS Bode plot reaches an impedance value that is twice the initially measured value at manufacture stage (coil's start of life). This threshold analysis by the change in the impedance profile is particularly significant for coil health assessment via the proposed analysis as a non-destructive inspection tool. For comparison with conventional tests, the examined coils received a "pass" outcome during Hi-POT testing at 4500 hours (before critical point) as well as at 5100 hours (near critical point) and at 5700 hours (after critical point).

The zones defined through the analysis of Fig. 4 are linked to the overall coil structure's health state after extensive thermal stresses, thus reflecting the health state of the insulation system made up from the individual components. The coil's "start of life zone" (Zone 1) reflects the period of as-manufactured coils or coils at 0 hours of thermal aging; in this zone the coils start to age with a prominent effect of the thermal exposure at increased rate lasting for approximately 1000 hours. The impedance profile of the coils' insulation system then enters the "main degradation zone" (Zone 2); this zone the lengthiest zone in terms of time span, however the thermal degradation effects are inflicted on the coils with a slower rate with the gradient of the curve decreasing. Although Zone 1 links to start of life and Zone 2 to the degrading period of the coil, in terms of insulation health both zones comprise the healthy state of the overall coil insulation system. These two make up the coil's useful life span of the degradation vs. frequency shift curves of Fig. 5. Further than these zones, the on-set of the critical points where the impedance profile starts reversing (gradient changes to negative) designate the "near-failure" zone condition in terms of the overall coil insulation health. From these points onwards, the coil enters the "end of life" zone in terms of the thermal stress effects initiating the insulation failure and its propagation.

The reverse behaviour in the impedance profile from the critical point onwards designates the failure and relates with the change in the coil inductance inflicted by the extended effect of thermal degradation beyond a stress endurance threshold. As the thermal degradation progresses, the encapsulation varnish (VPI) and the PAI-based coating insulation of the copper wire conductors diminishes in terms of dielectric strength, thermal endurance and mechanical adhesiveness. This diminishing mechanism is accelerated as the insulation aging nears the critical point area up to a point where there is a local loss of the latter two insulating components in several locations within a coil side. As such, the wire strands agglomerate locally with areas of strands coming in contact. Therefore, the inductance of the coil and the insulation system starts to decrease from the critical point onwards. This inflicts a drastic change in the impedance profile which reverses compared to the observed trend prior to the critical point. These findings provide further insight into the complete impedance profile up to the point of failure, thus rendering the critical point thresholds provided by Fig. 4 and Fig. 5 for identification of the ending of useful life and initiated failure. The discussed rationale for the inductance reduction during the failure occurrence is supported by the literature, where similar inductance reductions were discussed for cases of faulted coils and aged insulation systems in electrical machines [53]-[55], transformer windings [56]-[60] and wire fault location in coaxial cables [61]. Additionally, the effects of AC resistance, skin effects and proximity losses in Litz wire formed coils, reflected by reductions in the coil inductance, are discussed by physics-informed interpretations in [63]-[68]. The discussed degradation effects on the overall coil insulation system will also be shown through the next sections, validating these changes via inductance drops in

simulations and via equations (2)-(3), as well as by intrinsic inspection of the insulation system.

B. Validation via the Impedance Nyquist Plots

In tandem with the above analysis of the frequency responses, the impedance Nyquist plots are examined to visualise the trends of the real and imaginary components of the coil impedance. This plot is illustrated in Fig. 6. As in the case of Fig. 3, only the plots of C1 are shown as the analysis is the same for any coil. As described in [21], the circular or elliptical shape of the coil impedance locus is retained during thermal ageing, while it expands with the progression of the hours at temperature exposure. However, considering the profile plots over the ageing span presented in Fig. 4 and the lifing plots over frequency in Fig. 5, there is a certain point of degradation at which the locus ceases to expand. At that point, the locus reverses its behaviour and starts shrinking back to lower values of the real and imaginary components. These coincide with the critical points identified through Fig. 4 and Fig. 5 indicating the end of useful life in the coil due to the tangible change in the inductance, thus reversing the impedance profile. As with the critical points, the profile change occurs in the Nyquist plots is at 5600, 5700, 5500, and 4800 hours of thermal ageing for C1, C2, C3, C4, respectively. The key finding of this analysis combined with the lifespan plots of the previous section, is the identification of the actual failure profile due to thermal degradation effects. It is significant to note that the above analysis and thresholds pertain to the effects and ageing of thermal stresses only, whereas the effect of mechanical or other stresses is not considered in these laboratory conditions.

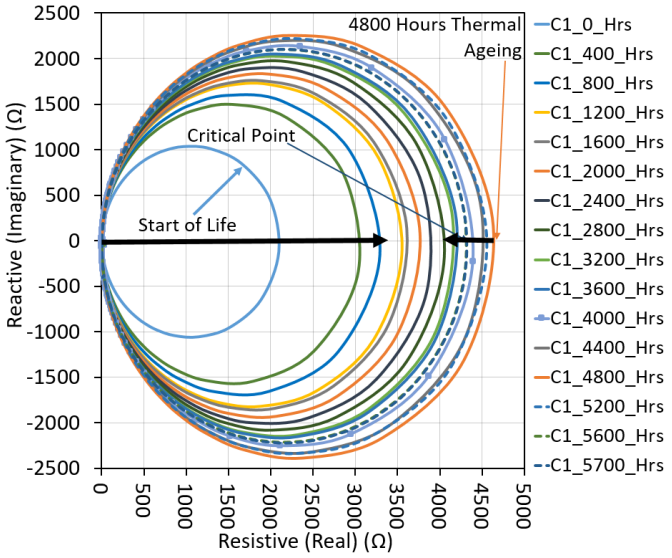

Fig. 6. Nyquist plots showing the evolution of the impedance locus and critical point where the locus reverses.

C. Validation via Simulations of Coil Impedance in Frequency Response Analysis (FRA)

In [28] and [62], an equivalent RLC circuit model was used as the electrical equivalent of a coil assembly to demonstrate the variability of the impedance via the Nyquist plots with the progression of aging by the consecutive capacitance drops per ageing cycle. In the latter study, this demonstrated the drops in the capacitance resulting in expansion of the Nyquist locus. In this work, the same corresponding RLC equivalent as in [28] and [62] was simulated to demonstrate the newly identified critical points validating the inductance drops that result in reversing the impedance profile. To this end, Fig. 7a shows the impedance FRA for the above coil equivalent reflecting consecutive changes in the capacitance (solid lines represent capacitance changes). The first peak change in the equivalent occurs when the capacitance drops from its initial value (C) to half (0.5C). From the peak illustrating the biggest capacitance drop onwards (at 0.25C), gradual changes in the inductance (dashed lines) are considered showing the impedance profile change that corresponds to the critical point identified via the experimental measurements due to the decreases taking place in the inductance of the coil. Furthermore, Fig. 7b depicts the impedance Nyquist plot, showing the locus expansion by capacitance drops (solid arrow) and then reversing its trend with the impedance profile change ensued by the inductance drops (dashed arrow).

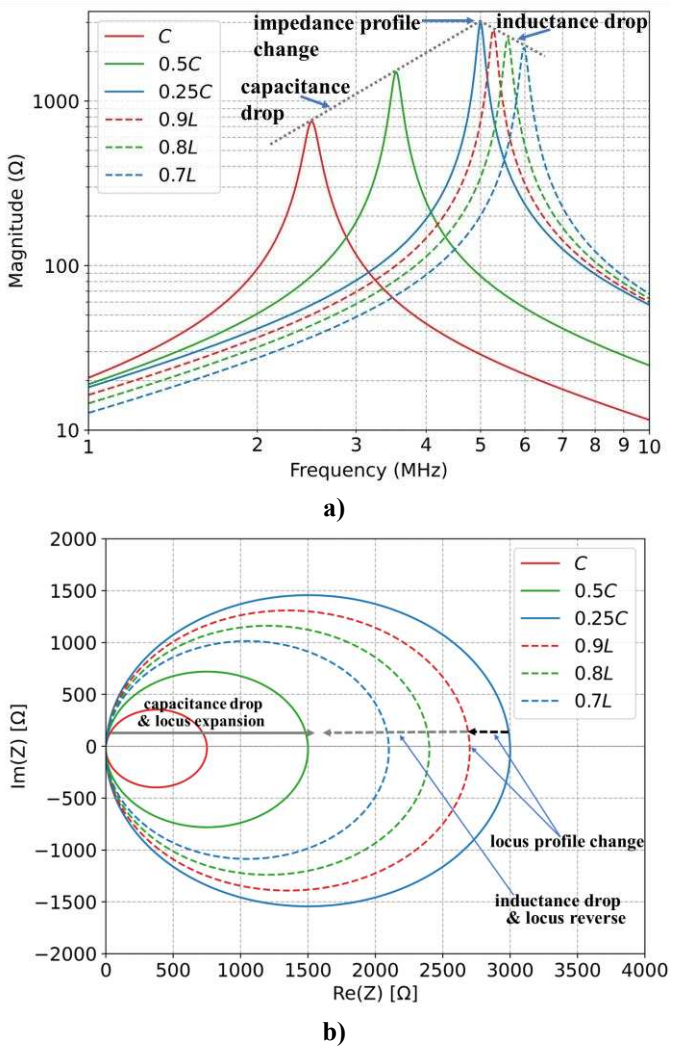

Fig. 7. Demonstration of changes in the impedance profile by the equivalent RCL due to changes in the capacitance and inductance: a) peak impedance tracking via the Bode plots and, and b) Nyquist locus and profile change. Baseline reference parameter values: R=2.5 Ω, L=2.75 μH, and C=1.47 nF.

As also explained by [27], the drops in the global capacitance of the coil result in the increase of the total impedance with the frequency f_{max} shifting to the higher end of the spectrum as shown in Fig. 7a. These capacitance changes correspond to the increasing impedance trendlines of Zone #1 and #2, reflecting the degradation profile and coil useful life as well as the expansion of the impedance Nyquist locus (Fig. 7b). The gradual drops in the inductance of the system correspond to the change in the impedance profile, which reverses demonstrating a decreasing trend that is opposite to the one prior to the critical point. This also corresponds to the Nyquist locus reversing its behaviour, shrinking back towards lower impedance values. These render by simulations the validation of the critical points and their interpretation, as discussed through Fig. 4 and Fig. 5.

D. Validation by Intrinsic Inspection with Microscopy and CT

For the physical validation of the discussed degradation effect and the interpretation of the failure mechanism through the identified critical points, this section provides a comparison of two coils during unaged stage and aged near to the critical point (~4500-4600 hours). This comparison is performed by intrinsic inspection with microscopy and tomography (CT scans). To this end, Fig. 8 shows the comparison of the microscopy view at 175x magnification of the interturn strands and encapsulation varnish. The healthy (unaged) VPI between the copper wire conductors is denoted with arrows in Fig. 8a. In Fig. 8b, the degradation effect and failure mechanism are seen by the evaporated VPI (circled) and agglomerated strands in several areas (dashed circles) as well as by the discoloration of the wire due to the diminished insulation coating.

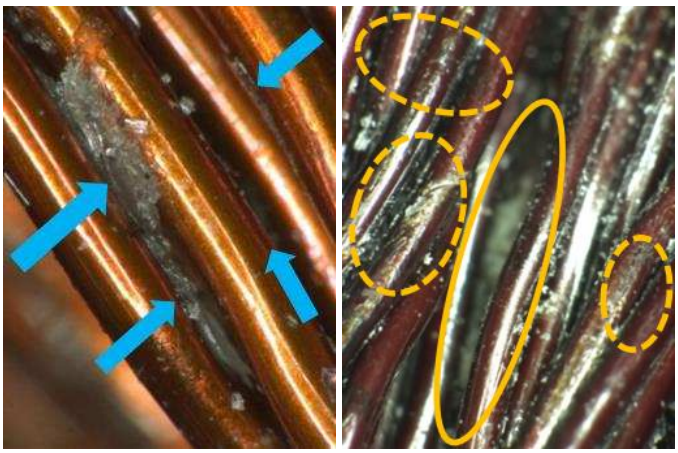

a) **b)**

Fig. 8. Microscopy view (175x magnification) of coil interturn strands and insulation layers: a) healthy (unaged) VPI, and b) coating degradation and missing VPI due to thermal aging.

For additional validation, the aged and unaged coil were subjected to CT scans. The tomography comparison is shown in Fig. 9, where the unaged insulation system is shown at the left side of each subfigure versus the aged one at the right. The arrows in left-side subfigures of Fig. 8a and 8b point to the areas of healthy unaged insulation system components, visible as areas with more shades. The arrows in the right-side subfigures of Fig. 8a and 8b show the progression of degradation and component loss in several areas due to the thermal stress, with notably less shaded areas over the coil sides. In Fig. 9c, the circles in the left-side subfigure show examples of areas within coil turns with healthy (unaged) wire coating and adequate penetration of the encapsulation varnish within strands. The circles in the right-side subfigure of Fig. 9c point to examples of areas where the discussed degradation mechanism has eliminated the latter two insulating components. This is due to thermal stress that to an extent that results in the failure initiation allowing the conductors to make contact. This failure mechanism accommodates the inductance drops beyond the critical point due to the fused conductors in several areas within bundle turns as shown in Fig. 9c (left), which results in the change of the impedance profile.

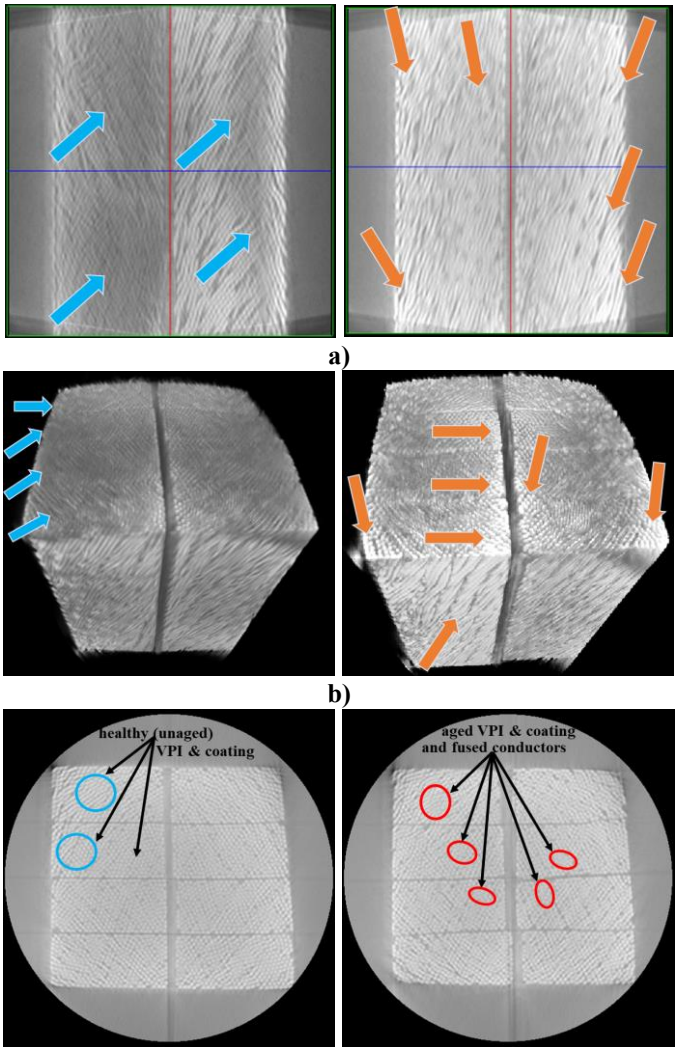

Fig. 9. Tomography comparison of unaged (left) versus aged (right) coil: a) top view of one coil side, b) side view of copper turn bundles, and c) front view of turns and copper strands area.

The observations drawn from the microscopy images of Fig. 8 and the CT scans of Fig. 9 point to the loss of insulating components within the coil insulation system due to components reaching their end-of-life stage after the identified critical point. These observations are linked with the drop in the overall coil impedance after the critical point, which is

attributed to the reduction of the coils' inductance at the end-of-life stages. The rationale for the decrease of inductance after the thermal failure point is also validated through Fig. 10. The latter figure depicts a magnification of the impedance frequency response in the frequency range of up to 100 kHz, demonstrating the decrease in the inductance when comparing the impedance profile before the thermal failure (blue line, at 5100 hours) and past the critical point while entering the failure zone (green curve, 5600 hours).

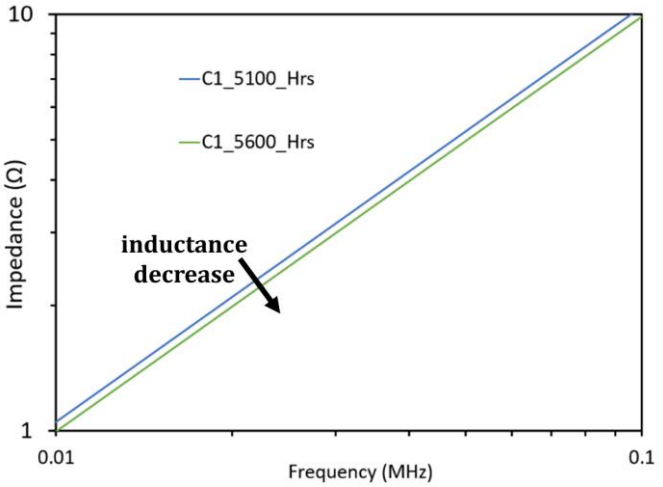

Fig. 10. Comparative impedance response of coil C1 up to 100kHz, before the critical point (5100 hours) and after the thermal failure (5600 hours) demonstrating the decrease of inductance due to insulating materials failure.

V. Conclusions

This paper presented a novel application of EIS for purposes of ex-situ inspection and health assessment of coils from a concentrated stator winding. Using the two key aspects of impedance spectroscopy, the frequency response of the Bode plots and the impedance locus of the Nyquist plots, the thermal degradation profile was mapped until the point of thermal failure. The monotonic behaviour of the impedance changes by the peak impedance tracking in the frequency responses. The trendline of these peaks and the failure mechanism were profiled with respect to the hours of ageing, as well as the resonant frequencies, for the first time until the point of thermal failure profiling, thus revealing critical points as indicators of the failure mechanism initiation under the sole effect of thermal stress. These profiles were used to identify key areas in the lifespan curve and critical lifespan points of the stator coil insulation system. The discussed results were validated by the well-known impedance Nyquist plots as well as by simulations and intrinsic inspection of the insulation system. These validations confirmed the critical points initiating a reverse behaviour of the locus with monotonic reduction of the real and imaginary components of the impedance. The impedance profiles were tracked and interpreted with respect to changes in the insulation system capacitance correlated with the progression of ageing. On the other hand, the initiation and mechanisms of the thermal failure only were interpreted and correlated with changes in the overall impedance profile due to changes in the inductance of the system from the critical points onwards. Such lifespan indicators enable a significant leap forward in the state of the art for remaining useful life prediction with a great potential to further enable a life estimation tool for coils insulation via impedance profiles. This is a key contribution of the presented work, as it identifies the critical points where the insulation failure is initiated and provides an interpretation of the failure with regards to the impedance profile change. The presented methodology is limited to concentrated stator coils using Litz wire in the coil turns, while further investigation is required for other types of windings and insulation grades.

Although the presented methodology for the identification of life thresholds has been thoroughly validated, the effects of solely thermal stresses were examined in this work. This is a significant contribution to the state of the art compared to existing studies. The proposed methodology maps the exact trendline of ageing and thermal failure profile under the gradual degradation effects at near rated temperature rather than accelerated stresses or accelerated thermal cycling that can compromise the behaviour of the impedance profile. Future work in this direction aims to map the effect of multi-stress factors such as electrothermal and electromechanical effects, or other combinations of T.E.A.M. stresses on the insulation system. Despite the limitation of evaluating thermal failure effects only, the approach presented in this work renders a technique to map the degradation profile of any individual stress type separated from other stresses, that affects the insulation system's material properties in a way that causes alterations in the impedance profile of coils and stator windings. Moreover, elements of future work to this direction ought to explore the evaluation of the potential impact of multi-stress effects on the presented life tool, as well as the establishment of a database to support degradation-informed coil insulation modelling that considers the effects of different stress types.

References

[1] Selema, A., Ibrahim, M. N., & Sergeant, P. (2022). Electrical machines winding technology: Latest advancements for transportation Electrification. Machines, 10(7), 563.

[2] Barzkar, A., & Ghassemi, M. (2022). Components of electrical power systems in more and all-electric aircraft: A review. IEEE Transactions on Transportation Electrification, 8(4), 4037-4053.

[3] Sayed, E., Abdalmagid, M., Pietrini, G., Sa'adeh, N. M., Callegaro, A. D., Goldstein, C., & Emadi, A. (2021). Review of electric machines in more-/hybrid-/turbo-electric aircraft. IEEE Transactions on Transportation Electrification, 7(4), 2976-3005.

[4] Petri, T., Keller, M., & Parspour, N. (2022). The insulation resilience of inverter-fed low voltage traction machines: Review, challenges, and opportunities. IEEE Access, 10, 104023-104049.

[5] Madonna, V., Giangrande, P., Lusuardi, L., Cavallini, A., Gerada, C., & Galea, M. (2019). Thermal overload and insulation aging of short duty cycle, aerospace motors. IEEE Transactions on Industrial Electronics, 67(4), 2618-2629.

[6] Madonna, V., Giangrande, P., & Galea, M. (2018). Electrical power generation in aircraft: Review, challenges, and opportunities. IEEE Transactions on Transportation Electrification, 4(3), 646-659.

[7] Panagiotou, P. A., Lambourne, A., & Jewell, G. W. (2022, September). Survey of insulation in electrical machines for aerospace: Systems, materials & inspection. In 2022 International Conference on Electrical Machines (ICEM) (pp. 2318-2324). IEEE.

[8] Saeed, M., Fernández, D., Guerrero, J. M., Díaz, I., & Briz, F. (2024). Insulation Condition Assessment in Inverter-Fed Motors Using the High-Frequency Common Mode Current: A Case Study. Energies, 17(2), 470.

[9] Verginadis, D., Antonino-Daviu, J. A., Karlis, A., & Danikas, M. G. (2021). Determination of the insulation condition in synchronous generators: Industrial methods and a case study. IEEE Industry Applications Magazine, 28(2), 67-77.

[10] Ruiz-Sarrio, J. E., Antonino-Daviu, J. A., Navarro-Navarro, A., & Biot-Monterde, V. (2023, August). Broadband Technique Analysis for Insulation Fault Detection and Condition Monitoring in Rotating Electrical Machines. In 2023 IEEE 14th International Symposium on Diagnostics for Electrical Machines, Power Electronics and Drives (SDEMPED) (pp. 574-580). IEEE.

[11] Vala, S. S., Mirza, A. B., Emon, A. I., & Luo, F. (2024). A Review of Partial Discharge in Stator Winding of Rotating Machines Fed by Voltage Source PWM Motor Drives. IEEE Transactions on Industry Applications.

[12] Ogundiran, Y. L., & Griffo, A. (2023, April). A Novel Modified Archimedes Spiral Antenna for Partial Discharge Detection in Inverter-Fed Electrical Machines. In 2023 IEEE Workshop on Electrical Machines Design, Control and Diagnosis (WEMDCD) (pp. 1-6). IEEE.

[13] Tsyokhla, I., Griffo, A., & Wang, J. (2015, May). On-line monitoring of winding insulation health using high frequency common mode voltage from PWM. In 2015 IEEE International Electric Machines & Drives Conference (IEMDC) (pp. 1433-1439). IEEE.

[14] Tsyokhla, I., Griffo, A., & Wang, J. (2019). Detection of humidity ingress using online common‐mode insulation impedance‐monitoring system. The Journal of Engineering, 2019(17), 4411-4414.

[15] Zheng, D., Lu, G., Wu, Y., Zhang, Q., & Zhang, P. (2023). Online Detection and Classification of Inter-turn and Groundwall Insulation Ageing based on Broadband Common-mode Impedance Spectrum. IEEE Transactions on Industrial Electronics.

[16] Ji, Y., Giangrande, P., Madonna, V., Zhao, W., Galea, M., Li, J., & Zhang, H. (2022, September). Investigation on Humidity Effect on Partial Discharge Considering Thermal Aging. In 2022 International Conference on Electrical Machines (ICEM) (pp. 2325-2330). IEEE.

[17] Panagiotou, P. A., Lambourne, A., & Jewell, G. W. (2022, September). Ex-situ Inspection of Concentrated Stator Coils by Means of Impedance Spectroscopy. In 2022 International Conference on Electrical Machines (ICEM) (pp. 2331-2337). IEEE.

[18] Lebey, T., Rumi, A., & Cavallini, A. (2022). Challenges for electrical insulation systems in high voltage aviation applications. IEEE Electrical Insulation Magazine, 38(6), 5-11.

[19] Borghei, M., & Ghassemi, M. (2021). Insulation materials and systems for more-and all-electric aircraft: A review identifying challenges and future research needs. IEEE Transactions on Transportation Electrification, 7(3), 1930-1953.

[20] Stone, G. C., Boulter, E. A., Culbert, I., & Dhirani, H. (2004). Electrical insulation for rotating machines: design, evaluation, aging, testing, and repair (Vol. 21). John Wiley & Sons.

[21] Panagiotou, P. A., Stone, E. J., Mühlthaler, J., Reeh, A., Lambourne, A., & Jewell, G. W. (2023, August). Thermal Degradation Profile of Concentrated Stator Winding Insulation by Impedance Spectroscopy. In 2023 IEEE 14th International Symposium on Diagnostics for Electrical Machines, Power Electronics and Drives (SDEMPED) (pp. 554-560).

[22] Delogu, G., Porru, M., & Serpi, A. (2021, October). A Brief Overview on Commercial Aircraft Electrification: Limits and Future Trends. In 2021 IEEE Vehicle Power and Propulsion Conference (VPPC) (pp. 1-5). IEEE.

[23] Trentin, A., Sala, G., Tarisciotti, L., Galassini, A., Degano, M., Connor, P.H., Golovanov, D., Gerada, D., Xu, Z., La Rocca, A. and Eastwick, C.N., 2020. Research and realization of high-power medium-voltage active rectifier concepts for future hybrid-electric aircraft generation. IEEE transactions on industrial electronics, 68(12), pp.11684-11695.

[24] Ghassemi, M., Barzkar, A., & Saghafi, M. (2022). All-Electric NASA N3-X aircraft electric power systems. IEEE Transactions on Transportation Electrification, 8(4), 4091-4104.

[25] FFd, S., Fernandes, J. F. P., & PJdC, B. (2021). Barriers and Challenges Going From Conventional to Cryogenic Superconducting Propulsion for Hybrid and All-Electric Aircrafts.

[26] Fard, M. T., & He, J. (2021, October). Comparison of medium-voltage high-frequency power inverters for aircraft propulsion drives. In 2021 IEEE Energy Conversion Congress and Exposition (ECCE) (pp. 1599-1605). IEEE.

[27] Stone, E. J., Panagiotou, P. A., Mühlthaler, J., Mills, A. R., Lambourne, A., & Jewell, G. W. (2024, September). Identification of Thermal Failure Profiles in Stator Winding Insulation by Impedance Spectroscopy. In 2024 International Conference on Electrical Machines (ICEM) (pp. 1-7).

[28] Stone, E.J., Panagiotou, P.A., Mühlthaler, J., Reeh, A., Lambourne, A. and Jewell, G.W., 2025. Thermal degradation profile mapping in stator coil insulation by impedance spectroscopy. IEEE Transactions on Industry Applications, Vol. 61, pp. 6110-6119.

[29] Rui, R., & Cotton, I. (2010, June). Impact of low pressure aerospace environment on machine winding insulation. In 2010 IEEE International Symposium on Electrical Insulation (pp. 1-5). IEEE.

[30] Mühlthaler, J., Lehner, B., Reeh, A., & Herzog, H. G. (2022, September). Search coil based detection of inter turn short circuit faults in permanent magnet synchronous machines. In 2022 International Conference on Electrical Machines (ICEM) (pp. 724-730). IEEE.

[31] Mühlthaler, J., Panagiotou, P. A., Lehner, B., Reeh, A., Herzog, H. G., & Gyftakis, K. N. (2023, August). Search Coil Based Detection of the Inter-Turn Short Circuits in Aircraft Permanent Magnet Synchronous Machine by Signal Frequency Extraction. In 2023 IEEE 14th International Symposium on Diagnostics for Electrical Machines, Power Electronics and Drives (SDEMPED) (pp. 76-82). IEEE.

[32] Gegenava, A., Khazanov, A. and Moore, B., 2016, June. Failure evaluation of the electrical insulation for high voltage stator windings machines and root cause analysis through visual inspection of dissected coils. In 2016 IEEE Electrical Insulation Conference (EIC) (pp. 404-408). IEEE.

[33] Leffler, J., & Trnka, P. (2022, July). Failures of Electrical Machines-Review. In 2022 8th International Youth Conference on Energy (IYCE) (pp. 1-4). IEEE.

[34] Khazanov, A., Gegenava, A., & Dawson, F. (2020, June). Considerations for maximum operational stresses in electrical insulation for high voltage machines stator windings for different rated voltages. In 2020 IEEE Electrical Insulation Conference (EIC) (pp. 54-57). IEEE.

[35] Gegenava, A., Khazanov, A., & Moore, B. (2017, June). Acceleration factors for faster Voltage Endurance Testing on generator insulation systems. In 2017 IEEE Electrical Insulation Conference (EIC) (pp. 177-180). IEEE.

[36] Gegenava, A., Khazanov, A., & Dawson, F. (2019, June). Corona in high voltage rotating machines stator. Causes, repair and prognosis. In 2019 IEEE Electrical Insulation Conference (EIC) (pp. 124-128). IEEE.

[37] Tanaka, T., & Imai, T. (2023, October). Recent Machine Learning-Based Studies of Electrical Insulation Technology. In 2023 IEEE Conference on Electrical Insulation and Dielectric Phenomena (CEIDP) (pp. 1-4). IEEE.

[38] Khazanov, A., & Gegenava, A. (2023, June). Step Increased Voltage Endurance Test as a Tool for Evaluation of Life Expectancy for Stator Windingb Ground Wall Insulation High Voltage Rotating Machines. In 2023 IEEE Electrical Insulation Conference (EIC) (pp. 1-5). IEEE.

[39] Han, Q., Chen, L., Cotton, I., & Khan, J. (2022). Insulating gases for partial discharge management of electrical machines in aerospace applications. IEEE Transactions on Transportation Electrification, 9(3), 3590-3600.

[40] Leuzzi, R., Monopoli, V. G., Rovere, L., Cupertino, F., & Zanchetta, P. (2019). Analysis and detection of electrical aging effects on high-speed motor insulation. IEEE Transactions on Industry Applications, 55(6), 6018-6025.

[41] Gegenava, A., & Khazanov, A. (2023, June). Statistical Review of Voltage Endurance Test of Insulation for High Voltage Rotating Machines Stator Windings with Combined Standard and Accelerated Tests.“Three Steps Test” TST. In 2023 IEEE Electrical Insulation Conference (EIC) (pp. 1-4). IEEE.

[42] Giangrande, P., Madonna, V., Nuzzo, S., & Galea, M. (2020). Moving toward a reliability-oriented design approach of low-voltage electrical machines by including insulation thermal aging considerations. IEEE Transactions on Transportation Electrification, 6(1), 16-27.

[43] Nahir, T.M., 2005. Impedance Spectroscopy: Theory, Experiment, and Applications, Edited by Evgenij Barsoukov (Texas Instruments Inc.) and J. Ross Macdonald (University of North Carolina, Chapel Hill). John Wiley & Sons, Inc.: Hoboken, NJ. 2005. ISBN 0471-64749-7.

[44] Shi, Q., & Kanoun, O. (2015). Wire fault diagnosis in the frequency domain by impedance spectroscopy. IEEE Transactions on Instrumentation and Measurement, 64(8), 2179-2187.

[45] Ciucci, F. (2019). Modeling electrochemical impedance spectroscopy. Current Opinion in Electrochemistry, 13, 132-139.

[46] Perisse, F., Werynski, P., & Roger, D. (2007). A new method for AC machine turn insulation diagnostic based on high frequency resonances. IEEE Transactions on Dielectrics and Electrical Insulation, 14(5), 1308-1315.

[47] Neti, P., & Grubic, S. (2016). Online broadband insulation spectroscopy of induction machines using signal injection. IEEE Transactions on Industry Applications, 53(2), 1054-1062.

[48] Ruiz-Sarrio, J. E., Chauvicourt, F., & Martis, C. (2022, September). Sensitivity analysis of a numerical high-frequency impedance model for rotating electrical machines. In 2022 International Conference on Electrical Machines (ICEM) (pp. 1260-1266). IEEE.

[49] Kavanagh, D. F., Howey, D. A., & McCulloch, M. D. (2013, August). An applied laboratory characterisation approach for electric machine insulation. In 2013 9th IEEE International Symposium on Diagnostics for Electric Machines, Power Electronics and Drives (SDEMPED) (pp. 391-395). IEEE.

[50] IEC 60034-27-3: "Rotating electrical machines Part 27-3 – Dielectric dissipation factor measurement on stator winding insulation of rotating electrical machines". 2015.

[51] IEC 60034-27-1: "Rotating eletctrical machines Part 27-1 – Off-line partial discharge measurements on the winding insulation". 2017.

[52] IEC 60034-15: "Impulse voltage withstand levels of form-wound stator coils for rotating a.c. machines". 2009.

[53] Jameson, N. J., Azarian, M. H., & Pecht, M. (2017). Impedance-based condition monitoring for insulation systems used in low-voltage electromagnetic coils. IEEE Transactions on Industrial Electronics, 64(5), 3748-3757.

[54] Zheng, D. and Zhang, P., 2019, September. An improved broadband common-mode electrical machine model for online condition monitoring of stator insulation degradation. In 2019 IEEE Energy Conversion Congress and Exposition (ECCE) (pp. 7012-7018). IEEE.

[55] Wang, K., Guo, H., Xu, A. and Pecht, M., 2020. Degradation monitoring of insulation systems used in low-voltage electromagnetic coils under thermal loading conditions from a creep point of view. Sensors, 20(13), p.3696.

[56] Banaszak, S., Gawrylczyk, K.M., Trela, K. and Bohatyrewicz, P., 2019. The Influence of Capacitance and Inductance Changes on Frequency Response of Transformer Windings. Applied Sciences, 9(5), p.1024.

[57] Podoltsev, A. D., Abeywickrama, K. N. B., Serdyuk, Y. V., & Gubanski, S. M. (2007). Multiscale computations of parameters of power transformer windings at high frequencies. Part I: Small-scale level. IEEE Transactions on magnetics, 43(11), 3991-3998.

[58] Podoltsev, A. D., Abeywickrama, K. N. B., Serdyuk, Y. V., & Gubanski, S. M. (2007). Multiscale computations of parameters of power transformer windings at high frequencies. Part II: Large-scale level. IEEE Transactions on Magnetics, 43(12), 4076-4082.

[59] Gawrylczyk, K. M., & Trela, K. (2019). Frequency response modeling of transformer windings utilizing the equivalent parameters of a laminated core. Energies, 12(12), 2371.

[60] Fofana, I., & Hadjadj, Y. (2016). Electrical-based diagnostic techniques for assessing insulation condition in aged transformers. Energies, 9(9), 679.

[61] Shi, Q., & Kanoun, O. (2013). Wire fault location in coaxial cables by impedance spectroscopy. IEEE Sensors Journal, 13(11), 4465-4473.

[62] E. J. W. Stone, P. A. Panagiotou, J. Mühlthaler, A. R. Mills, A. Lambourne and G. W. Jewell, "Modelling of Insulation in Concentrated Stator Coils for Characterisation and Material Changes," 2024 International Conference on Electrical Machines (ICEM), Torino, Italy, 2024, pp. 01-08, doi: 10.1109/ICEM60801.2024.10700317.

[63] Holloway, C.L., Kuester, E.F., Ruehli, A.E. and Antonini, G., 2013. Partial and internal inductance: Two of Clayton R. Paul's many passions. IEEE Transactions on Electromagnetic Compatibility, 55(4), pp.600-613.

[64] Capelli, F. and Riba, J.R., 2017. Analysis of formulas to calculate the AC inductance of different configurations of nonmagnetic circular conductors. Electrical Engineering, 99(3), pp.827-837.

[65] Nia, M.S.S., Saadatmand, S., Altimania, M., Shamsi, P. and Ferdowsi, M., 2019, October. Analysis of skin effect in high frequency isolation transformers. In 2019 North American Power Symposium (NAPS) (pp. 1-6). IEEE.

[66] Reatti, A. and Grasso, F., 2000, August. Solid and Litz-wire winding non-linear resistance comparison. In Proceedings of the 43rd IEEE Midwest Symposium on Circuits and Systems (Cat. No. CH37144) (Vol. 1, pp. 466-469). IEEE.

[67] Marzec, T.J., Grainger, B.M., Raju, R. and Ohodnicki, P.R., 2024. Analytical Models for Solid & Litz Wire AC Winding Loss in Toroidal Inductors. IEEE Transactions on Transportation Electrification.

[68] Tang, X. and Sullivan, C.R., 2003, June. Stranded wire with uninsulated strands as a low-cost alternative to litz wire. In IEEE 34th Annual Conference on Power Electronics Specialist, 2003. PESC'03. (Vol. 1, pp. 289-295). IEEE.

Edward J. W. Stone received the B.Eng. degree in electrical engineering from Sheffield Hallam University, Sheffield, U.K., in 2016, and the Ph.D. degree in synchronous reluctance machines from the Department of Electronic and Electrical Engineering of the University of Sheffield, Sheffield, U.K., in 2021.

Since receiving his Ph.D. degree in 2021, he is a Postdoctoral Research Associate with the Electrical Machines and Drives research group of the School of Electrical and Electronic Engineering of the University of Sheffield, Sheffield, U.K., working at the Rolls-Royce University Technology Centre in Advanced Electrical Machines of the University of Sheffield. His research interests include electrical machine design, Class D amplification, insulation monitoring and degradation, as well as inspection and repair technologies for electrical machines.

Dr. Stone is a member of the Institution of Engineering and Technology (IET, U.K.).

Panagiotis A. Panagiotou (M'22) received the 5-year Diploma (B.Eng. & M.Eng.) from the Department of Electrical and Computer Engineering of the University of Patras, Patras, Greece, in 2015, and the M.Sc. degree in Complex Systems and Network Theory from the Department of Mathematics of the Aristotle University of Thessaloniki, Thessaloniki, Greece, in 2017. He received the Ph.D. degree in fault diagnostics of electrical machines from Coventry University, Coventry, U.K., in 2020.

In 2021, he joined the Department of Electronic and Electrical Engineering of the University of Sheffield, Sheffield, U.K., as a postdoctoral research associate at the Rolls-Royce University Technology Centre for Advanced Electrical Machines of the University of Sheffield. Since 2022, he is a Lecturer in electrical machines with the School of Electrical and Electronic Engineering of the University of Sheffield, Sheffield, U.K. His research interests include condition monitoring, fault detection and diagnostics in electrical machines, signal processing for diagnostics, and technologies for the inspection and repair of electrical machines.

Dr. Panagiotou is a member of the IEEE, a member of the Institution of Engineering and Technology (IET, U.K.) and a Fellow of the Higher Education Academy (FHEA), U.K.

Johannes Mühlthaler (Member, IEEE, 2024) received the B.Eng. degree in electrical engineering from the University of Applied Sciences, Rosenheim, Germany, in 2017, and the M.Sc. degree in electrical engineering from the Technical University of Munich, Munich, Germany, in 2020.

In 2019, he joined Rolls-Royce Electrical Ltd & Co KG in Munich, Germany where he is currently a doctoral candidate working toward the Ph.D. degree with Technical University of Munich, Munich, Germany, and Rolls-Royce Electrical Ltd. & Co. Deutschland in Munich, Germany. His current research focuses on the modelling and verification of winding fault effects, fault detection and mitigation strategies in multi-lane permanent magnet synchronous machines.

Andrew R. Mills received the MEng degree in control systems and the PhD degree in control and monitoring system engineering from the University of Sheffield, Sheffield, UK, in 2003 and 2013, respectively. After working in the defense industry, he was a Senior Research Fellow at the University of Sheffield with a portfolio of aerospace research in application systems engineering, sensing and data-driven decision making to the application of safety-critical system through-life optimization.

Since 2025 he is a professor of Innovation in Aerospace Systems Monitoring and Control with the School of Electrical and Electronic Engineering of the University of Sheffield. He is the deputy director of the University of Sheffield Rolls-Royce University Technology Centre in Controls and Systems Engineering which seeks to use control systems engineering principles to a broad range of applied control and health management research challenges.

Alexis Lambourne received the B.Eng. degree in materials engineering from Loughborough University, U.K., in 1999 and the Ph.D. degree from Oxford University, Oxford, U.K., in 2003. He joined Rolls-Royce Submarines in 2003, and since 2005 he has been working for Rolls-Royce Plc. Central Technologies as a materials specialist in novel and emerging materials technologies.

From 2014-2017, he held a Royal Society industrial fellowship on the materials challenges for hybrid aerospace. His research focuses on the materials and manufacturing of high-power density electrical systems in aerospace environments, including materials selection, testing, degradation, inspection, and recycling. His research interests include a wide variety of functional, smart, and nano materials as well as their applications in aerospace and electric power systems.

Geraint W. Jewell received the B.Eng. and Ph.D. degrees in electrical engineering from the University of Sheffield, Sheffield, U.K., in 1988 and 1992, respectively. Since 1994, he has been a member of the academic staff with the School of Electrical and Electronic Engineering of the University of Sheffield, where he is a professor of electrical engineering.

He held an Engineering and Physical Sciences Research Council (EPSRC) Advanced Research Fellowship from 2000 to 2005 and a Royal Society Industry Fellowship with Rolls-Royce from 2006 to 2008. He is currently the director at the Rolls-Royce University Centre in Advanced Electrical Machines of the University of Sheffield, and the director at the EPSRC Future Electrical Machines Manufacturing Hub. His research interests include the modelling and design of a wide variety of electromagnetic devices, notably electrical machines for aerospace, electro-mechanical actuators, and high-temperature applications.